Title

Machine-Learning Enhanced AVA Inversion for Flow Model Generation

ISBN

9789462822894

Authors

Hoversten, GM

Chen, J

Commer, M

Publication Date

2019

DOI

10.3997/2214-4609.201901611

Peer reviewed

Introduction

Seismic AVA inversion is commonly used to develop reservoir models with the goal of producing detailed fine-scale permeability fields that can accurately represent the observed production data. The typical workflow transforms course-scale geophysical parameters, θ_c (acoustic velocity V_p, shear velocity V_s, density ρ, and porosity ϕ), derived from some form of AVA inversion through a rock physics model derived from log data to a fine-scale permeability model, k_f. Sulistiono et al. (2015) describes a commonly used work flow using current geostatistical inversion and statistical rock physics to produce an initial k_f model that then requires history matching to produce a final model. Once history matching has been done the new k_f model, when transformed back to θ_c, rarely fits the seismic data. In most cases the loop is not closed by cycling between AVA and production models until a common model is found that fits both the seismic and production data. Even if the loop is closed it requires considerable time and computing resources.

New developments in machine learning (ML) technology have provided methods that can link the course-scale θ_c to fine-scale k_f. However, unlike facial recognition applications where ML has performed well, ML applications in the earth sciences are limited by a relative lack of training data (a company may have 10's of seismic data sets compared to millions of photographs of faces in a facial recognition data base). The lack of real data examples can be ameliorated using the method of transfer-learning (Goodfellow, et al. 2016) where models and synthetic data are used to produce synthetic data for ML training.

Borrowing from the transfer-learning approach, we present a combination of stochastic MCMC-based AVA inversion (Hoversten et al. 2017) with conditional generative adversarial networks (cGAN). The starting point is a Bayesian model for full joint AVA and production data inversion. In this paper we use a simplified form of the complete model to develop a workflow that generates an ensemble of θ_c and k_f models that fit both the AVA data and the production data.

Method

The Bayesian model for the joint posterior distribution of $\boldsymbol{\theta_c}$ and $\boldsymbol{k_f}$, $\boldsymbol{f(\theta_c, k_f|S, D)}$, given AVA data (S) and production data (D) is given by

$$\boldsymbol{f(\theta_c, k_f|S, D) \propto f(S|\theta_c) \times f(D|k_f) \times f(k_f|\theta_c) \times f(\theta_c)} \quad (1)$$

where $\boldsymbol{f(S|\theta_c)}$ is the likelihood of S given $\boldsymbol{\theta_c}$ and $\boldsymbol{f(D|k_f)}$ is the likelihood of D given $\boldsymbol{k_f}$. The term that integrates cGAN into the stochastic inversion is $\boldsymbol{f(k_f|\theta_c)}$, the conditional probability of $\boldsymbol{k_f}$ given $\boldsymbol{\theta_c}$. The final term in (1) is the prior information on the probability of $\boldsymbol{\theta_c}$. The standalone stochastic AVA inversion (Hoversten et al. 2017) would remove $\boldsymbol{f(D|k_f)}$ and $\boldsymbol{f(k_f|\theta_c)}$ from the right-hand side leaving only the posterior $\boldsymbol{f(\theta_c|S)}$.

We have chosen cGAN to generate $\boldsymbol{f(k_f|\theta_c)}$ because it is currently under investigation by many researchers, leading to open source code that could be quickly tested and modified. The original Torch code developed by Isola et al. (2017) was tested and then modified for use in this work. Two options for the generator were considered: 1) Encoder-decoder networks (Hinton and Salakhutdinov, 2006, Badrinarayanan et al., 2016), and 2) U-net (Ronneberger et al., 2015). Further, two options for the discrimination were considered, 1) Markovian discriminator (PatchGAN) (Li and Ward, 2016), and 2) Conventional neural networks with variable layers. The choice of options is part of the model selection process. For the results shown here we chose U-net as the generator and conventional neural networks as the discriminator. The tuning parameter values were taken from Isola et al. (2017).

Equation (1) represents a full joint inversion of AVA and production data. For the AVA inversion, the forward problem required to evaluate $\boldsymbol{f}(\boldsymbol{S}|\boldsymbol{\theta_c})$ at each element of the Markov chain is a convolution that is fast, however the forward problem required to evaluate $\boldsymbol{f}(\boldsymbol{D}|\boldsymbol{k_f})$ is a flow simulation that is numerically intensive. While this is not impossible, and the end-product may justify the cost, we are investigating ways to speed the evaluation of $\boldsymbol{f}(\boldsymbol{D}|\boldsymbol{k_f})$**.** Approximations such as stream line simulation or emulation and even ML are being considered. In this presentation, we make the approximation that $\boldsymbol{f}(\boldsymbol{k_f}|\boldsymbol{\theta_c})$ is smaller than $\boldsymbol{f}(\boldsymbol{S}|\boldsymbol{\theta_c})$, allowing $\boldsymbol{f}(\boldsymbol{k_f}|\boldsymbol{\theta_c})$ to be dropped and thus decoupling $\boldsymbol{f}(\boldsymbol{D}|\boldsymbol{k_f})$ and $\boldsymbol{f}(\boldsymbol{S}|\boldsymbol{\theta_c})$**.** This results in a workflow that eliminates evaluation of $\boldsymbol{f}(\boldsymbol{k_f}|\boldsymbol{\theta_c})$ during the MCMC sampling and moves it to a post-inversion step, thus reducing the number of simulations required.

The process is summarized in five steps;

1) Numerical models based on flow simulations and rock-physics provide synthetic AVA data from $\boldsymbol{k_f}$ models.
2) Stochastic AVA inversion of the synthetic data from 1) provides an ensemble of course-scale $\boldsymbol{\theta_c}$ (i.e. V_p, V_s, ρ, ϕ) models.
3) cGAN is trained on the synthetic $\boldsymbol{\theta_c}$ and $\boldsymbol{k_f}$ to produce $\boldsymbol{f}(\boldsymbol{k_f}|\boldsymbol{\theta_c})$**.**
4) Field data is inverted and the conditional probability $\boldsymbol{f}(\boldsymbol{k_f}|\boldsymbol{\theta_c})$ is applied to the ensemble of stochastic $\boldsymbol{\theta_c}$ models producing an ensemble of $\boldsymbol{k_f}$ models.
5) All or a subset of the ensemble of $\boldsymbol{k_f}$ models have production simulated, and the models that match the field production data within the estimated variance are selected.

Steps 1-3 represent the transfer learning using models to generating training data and training the cGAN network. Step 4 provides an ensemble of $\boldsymbol{k_f}$ models that can be used as is or as input to step 5. Step 5 refines $\boldsymbol{k_f}$ to those that fit available production data. In the best-case scenario $\boldsymbol{k_f}$ models from step 5 may be used directly for production predictions; however, it is likely that these models will still require human interaction before they are field-ready. Nevertheless, our goal is to significantly accelerate the workflow and provide more robust $\boldsymbol{k_f}$ models compared to starting directly from rock-physics transformation of the course-scale $\boldsymbol{\theta_c}$.

Examples

To test the proposed inversion workflow, a fine-scale dual-permeability model that had previously been built for CO_2 injection modelling was used. The $\boldsymbol{k_f}$ field was generated using a first order Markov random field with horizontal and vertical weights calculated using an exponential variogram with correlation lengths of 25m and 0.5m in x and z directions, respectively. The permeability field was transformed to $\boldsymbol{\theta_c}$ using the rock-physics properties derived from a borehole used by Chen and Hoversten (2012).

Synthetic AVA gathers at 4ms sampling were generated every 16 meters on a 2D section. The synthetic data was first inverted for course-scale $\boldsymbol{\theta_c}$ using the algorithm from Hoversten et al. (2017). Figure 1 shows the true fine-scale permeability model, $\boldsymbol{k_f}$, the course-scale permeability, $\boldsymbol{k_c}$, converted from the median $\boldsymbol{\theta_c}$, an example synthetic angle gather used as observed data and the computed angle gather from the median $\boldsymbol{\theta_c}$ model.

Flow was modelled for a CO_2 injection well at the left side and production at the right side. In addition to the injection flow rate, the pressure and CO_2 saturation was also calculated at x of 128, 256, and 384 m at five depths from 43 to 213m to simulate monitor wells. In step 5) several combinations of injection flow rate, measured pressure and saturation were tested. Figure 2 shows the injection flow rate at the left side of the model, the pressure curves at x=256, z=1373m for 600 realizations of step 4), the MAP model from 600 realizations from step 4, and the $\boldsymbol{k_f}$ that best fits the 15 monitor pressure curves (step 5). In Figure 2a) and b) the pressure curve from the model derived from the course-scale AVA inversion without application of $\boldsymbol{f}(\boldsymbol{k_f}|\boldsymbol{\theta_c})$ (red curve) does a very poor job of fitting the observed flow rate and

pressures curve. This is true at all the pressure monitor locations and represents a common occurrence after AVA models are converted to flow models. The MAP solution from the 600 fine-scale realizations of step 4) without conditioning to the flow rate or pressure data (blue curve) is significantly closer to the true response (green curve) than that produced directly from the median $\boldsymbol{\theta_c}$ (red curve). If the 15 monitor locations are used in step 5) the best overall fits to observed pressure or saturation come from using the pressure or saturation respectively. The pressure responses from conditioning to the saturation data only (magenta), while better than AVA only, still has significant error in flow rate and pressure (Figure 2a and 2b) compared to conditioning to pressure data.

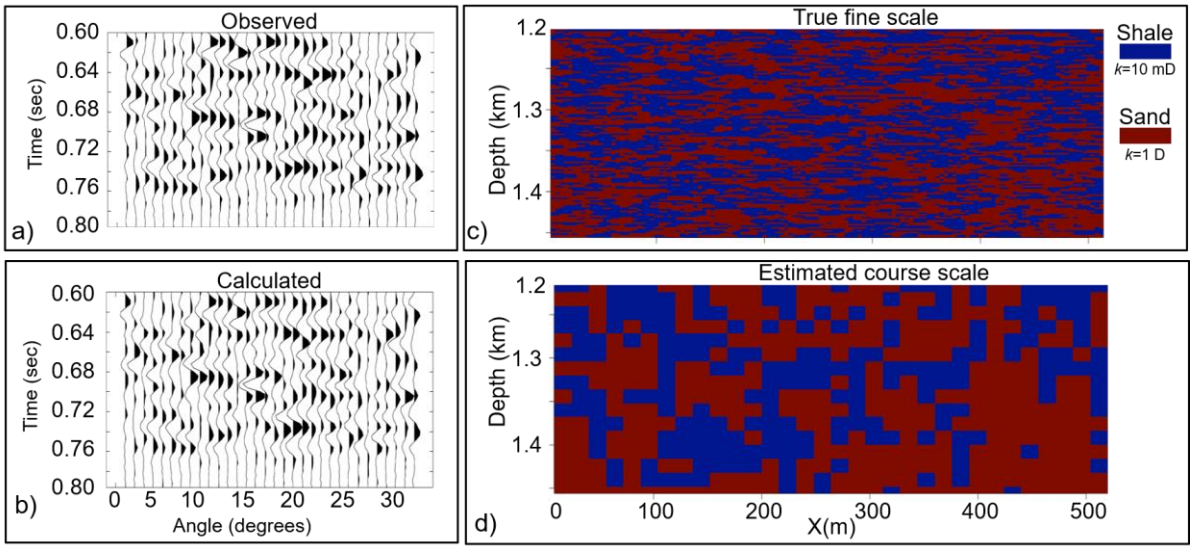

Figure 1 *a) A single angle gather from the true fine-scale model, b) the calculated gather from the median θ_c model from AVA inversion, c) the true fine-scale k_f model, d) the k model transformed from the median θ_c mode1 derived from AVA inversion. The fine-scale model has dx=4m, dz=2m, the inversion model has dx=16m, dz = 16m*

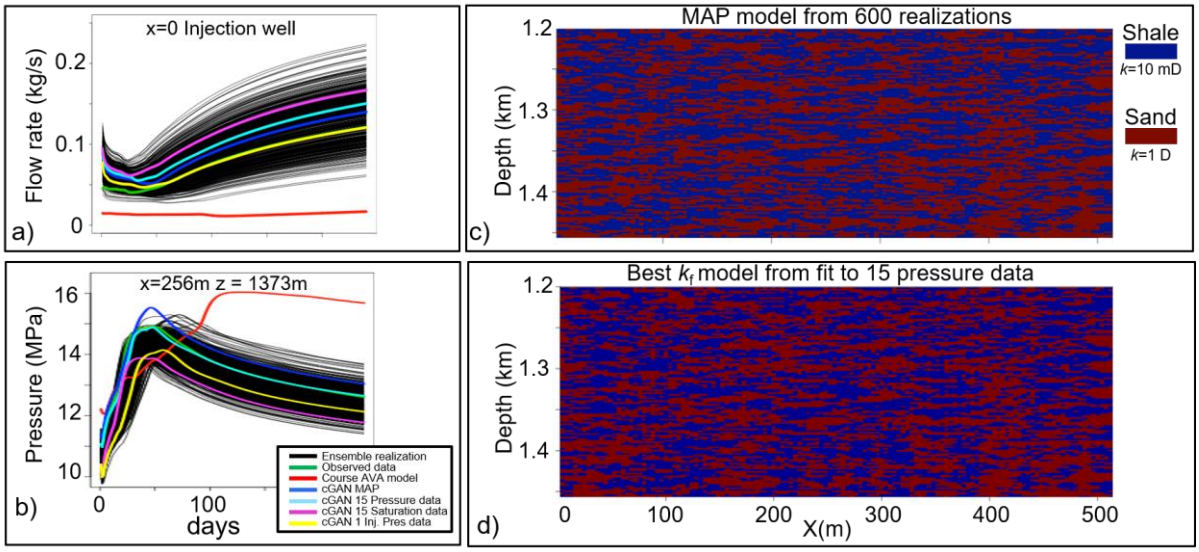

Figure 2 *a) flow rate at CO_2 injection well on left side of model, b) pressure at z=1373m in middle monitor well, c) MAP solution from the 600 fine-scale realizations of step 4) without conditioning to the flow rate or pressure data, d) k_f from best fit to 15 monitor-well pressure curves.*

While the spacing of the monitor wells in this model may be close to appropriate for mature land-based fields, in an offshore setting it is more likely that only a few wells would provide data. In the case here where only the injection flow rate is used in step 5, the $\boldsymbol{k_f}$ that best fits the flow rate data (yellow curve

in figure 2a) does a reasonable job of fitting the pressure at the monitor well locations (Figure 2b) and saturation (not shown) at the monitor locations.

Conclusions

In this study, we develop a new approach that bridges the gap between the resolution of seismic AVA inversion models and the fine-scale models required to match production data by combining Bayesian models with deep learning. Tests show that application of cGAN conditional probabilities applied to AVA-generated course-scale models significantly improves production history matches without additional flow simulations. Further, flow simulation of the ensemble of fine-scale models generated by cGAN conditional probabilities applied to AVA-generated course-scale parameters followed by selection of those models that best fit production data provides additional significant improvement. Since seismic inversion, training of the deep neural networks, and forward flow simulation are carried out separately, the workflow is scalable and can be applied to large-scale problems.

This work represents only a proof of concept, work continues to enhance many aspects of the workflow. In particular, the large number of tuneable parameters that control the performance of the cGAN network means that our choices are almost certainly not optimal. We observe that the spatial frequency content of the produced $\boldsymbol{k_f}$ models is somewhat higher than that of the true model. This is most likely due to sub-optimal cGAN parameter choices. Additionally, we are investigating ways to build constraints such as connectivity and/or lithotype ratios into the cGAN.

We are currently working on field data examples to test the current and enhanced workflows. We will report on the application to field data in 2019.

References

Chen, J. and Hoversten, G.M. [2012], Joint inversion of marine seismic AVA and CSEM data using statistical rock-physics models and Markov random fields: Geophysics, 77 , **1**, R65-R80.

Goodfellow, I., Bengio, Y., and Courville, A. [2016] Deep Learning. MIT Press, Cambridge, MA.

Hinton, G.E., and Salakhutdinov, R.R. [2006] Reducing the Dimensionality of Data with Neural Networks. Science, **323**, 504 – 507.

Hoversten G.M., Royle, A., Chen, J., Myer, D. [2017] MCMC Inversion of Offshore West Africa AVA Data. 79th EAGE Conference and Exhibition. **DOI:** 10.3997/2214-4609.201700545.

Isola, P., Zhu, J., Zhou, T., and Efros, A.A. [2017] Image-to-Image Translation with Conditional Adversarial Networks. CVPR 2017.

Li, C., Wand, M. [2016] Precomputed real-time texture synthesis with Markovian generative adversarial networks. In: ECCV

Ronneberger, O., Fischer, P., and Brox, T. [2015] U-net: Convolutional networks for biomedical image segmentation. In MICCAI, volume 9351, pp. 234–241.

Sulistiono, D., Vaughan, R., Ali, M., and Rasoulzadeh, S. [2015] Integrating Seismic and Well Data into Highly Detailed Reservoir Model through AVA Geostatistical Inversion. Abu Dhabi International Petroleum Exhibition and Conference 9-12 November 2015, SPE-177963-MS